ACS APPLIED MATERIALS & INTERFACES

Research Article

www.acsami.org

Fabrication of Structured Porous Films by Breath Figures and Phase Separation Processes: Tuning the Chemistry and Morphology Inside the Pores Using Click Chemistry

Alberto S. de León,[†] Adolfo del Campo,[‡] Marta Fernández-García,[†] Juan Rodríguez-Hernández,*[,†] and Alexandra Muñoz-Bonilla*[,†]

[†]Instituto de Ciencia y Tecnología de Polímeros (ICTP-CSIC), C/Juan de la Cierva 3, 28006-Madrid, Spain

[‡]Instituto de Cerámica y Vidrio (ICV-CSIC), C/Kelsen 5, 28049-Madrid, Spain

ABSTRACT: Herein, a facile water-assisted templating technique, the so-called breath figures method, in combination with phase separation process, was employed to prepare multifunctional micropatterned films. Tetrahydrofuran solutions of incompatible ternary blends consisting of high-molecular-weight polystyrene, an amphiphilic block copolymer, polystyrene-*b*-poly[poly(ethylene glycol) methyl ether methacrylate] (PS_{40}-*b*-$P(PEGMA300)_{48}$), and a fluorinated homopolymer, poly(2,3,4,5,6-pentafluorostyrene) ($P5FS_{21}$) were casted under humid atmosphere varying the proportion of the components. Two simultaneously occurring processes, i.e., the breath figures mechanism and the phase separation process, lead to unprecedented morphologies that could be tuned by simply varying the relative humidity or the composition of the blend. Confocal micro-Raman spectroscopy served to provide information about the location and distribution of the different functionalities in the films. As a result, both the amphiphilic block copolymer and the fluorinated polymer were mainly located in the cavities. Above a certain percentage of relative humidity, honeycomb structured films were obtained in which the block copolymer is distributed on the edge of the pore as a result of the affinity by the condensing water droplet and the coffee stain effect. The homopolymer is also preferentially situated at the pore edge, but forming spherical domains with narrow polydisperse sizes. Moreover, thiolated glucose molecules were specifically attached to the $P5FS_{21}$ domains via thiol-*para* fluorine "click" reaction. Subsequently, the specific lectin (Concanavalin A, *Canavalia ensiformis*) was attached to the surface by conjugation with the glucose moieties. The successful binding of the Con A was demonstrated by the fluorescence, observed exclusively at the areas where $P5FS_{21}$ domains are located. This nonlithographic method opens a new route to fabricate a huge variety of microstructured polymer films in terms of morphology not only for protein patterning, as illustrated in this manuscript, but also to produce a diversity of functional group arrangements.

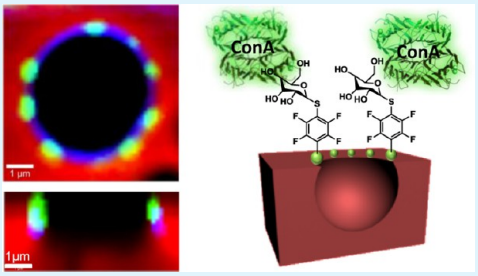

KEYWORDS: *breath figures, polymer blends, porous interfaces, click chemistry, phase separation, polymer surfaces*

INTRODUCTION

In recent years, there has been a growing interest in the fabrication of micropatterned polymer surfaces mainly due to their potential applications as templates, membranes, catalytic systems or sensors.[1−4] The design of surfaces with controlled topography is important in order to obtain new materials for the different applications. In most of the cases, the fabrication of microstructured polymer films involves top-down or bottom-up approaches mainly using both lithographic techniques and self-assembly processes. As an alternative, a dynamic templating method commonly called breath figures has been extensively applied to create microporous polymer films with well-ordered honeycomb structures.[5−10]

This technique uses water droplets as dynamic template and is based on the condensation of water vapor on the surface of a polymer solution during the solvent evaporation. Upon complete solvent and water evaporation, porous films can be obtained. One of the main advantages of this technique is, thus, the easy elimination of the template as the water droplets evaporate after forming the films. Varying the initial conditions, i.e., temperature, polymer concentration, solvent, or relative humidity, we can modify the size, shape, and distribution of the pores, obtaining more or less regular patterns.[11−13] Furthermore, the breath figures formation mechanism that involves precipitation of the polymers around the water droplets implies, in the case of amphiphilic structures, the orientation of the hydrophilic groups preferentially to the wall of the holes. Consequently, the chemical functionality of the cavities can be controlled simultaneously with the topography.[14−17] These ordered porous structures with controlled surface functionality exhibit potential in applications such as cell culturing, as microreactors or even as catalytic substrates.[18−20] In this sense, compared to other studies in which only a single functional copolymer has been employed, the use of polymeric blends

Received: February 22, 2013
Accepted: April 1, 2013
Published: April 1, 2013

consisting of functional polymers embedded into polymer matrix favors the preferential location of certain functionalities inside the cavities while the rest of the surface is formed almost exclusively by the polymer matrix; thus, controlling the functional group distribution. Our group has been involved in the fabrication of functional and multifunctional microstructured porous films via breath figures from blends of polymers.[14,21−23] The mixture of amphiphilic copolymers or functional homopolymers into a hydrophobic polymer matrix is an interesting approach to create honeycomb structures with functional cavities because of the combined action of the breath figures and the phase separation processes.[24−26] As has been recently reported, the use of ternary polymer blends results in unprecedented structured and multifunctional surfaces in a single step. However, the complexity of the systems significantly augments and, then, a careful design is required. Previously, a ternary blend of a high molecular weight polystyrene matrix mixed with two block copolymers, $P5FS_{21}$-*b*-PS_{31} and PS_{40}-*b*-$P(PEGMA300)_{48}$, were employed to prepare multifunctional and hierarchically structured porous patterned films.[23] In this case, the pores were enriched in PS_{40}-*b*-$P(PEGMA300)_{48}$ amphiphilic copolymer while the fluorinated copolymer remained homogeneously mixed with the PS matrix. Herein we investigated the patterned films obtained from a ternary polymer blend based on the PS matrix, PS_{40}-*b*-$P(PEGMA300)_{48}$ amphiphilic copolymer and a poly(2,3,4,5,6-pentafluorostyrene) homopolymer, ($P5FS_{21}$) instead of a diblock copolymer. In this case, $P5FS_{21}$ is supposed to be incompatible with the PS matrix because of the absence of the polystyrene segment of the block copolymer. Therefore, in the present article, we study the topography and the chemical distribution of the different polymers that form the microstructured films obtained by the combination of breath figures and the phase separation of incompatible polymers.

Moreover, the use of polymers with functional groups gives the possibility to introduce a wide range of functionalities on the breath figures pattern via postmodification reactions. For instance, Russell et al.[27] were pioneers in this sense, decorating the cavities with ligand-stabilized CdSe nanoparticles to further modify the surface functionality within the holes by simple chemical modification. In the current article, we took advantage of the "click" chemistry onto the functional fluorinated domains in order to illustrate the possibility to modify the functionality of the films. The concept of "click" chemistry was introduced in 2001 for highly efficient organic reactions,[28−31] and over the past decade has attracted an increasing interest and has been extended to the design and synthesis of novel macromolecular systems. One of the most attractive reactions is the so-called thiol-*para*-fluorine "click" reaction.[32,33] The labile *para*-fluorine substituent of pentafluorophenyl group can undergo nucleophilic substitution reaction with nucleophiles, such as thiols, under mild experimental conditions in a very efficient and selective way.[34] In particular, the use of glucose derivatives could be of interest among others to modify the surface for biomedical purposes. As will be described below, herein we employed acetylated β-D-thioglucopyranose as an example to be coupled onto the $P5FS_{21}$ regions of the microstructured films. Specific domains with attached glucose molecules can be obtained by using this reaction. Carbohydrates have been employed to illustrate the immobilization of the functional surface since they are involved in many biological recognition events through specific interactions with proteins such as enzymes or lectins.[35,36] The immobilization of carbohydrates only on the fluorinated domains of the microstructured polymer films provides a suitable template for patterning proteins, leading a powerful tool, for example, in the study of cell adhesion or even as biosensors. Several articles are reported in literature concerning the micropatterning of protein on breath figures films.[22,37−40] However, in most of the cases, the proteins are attached within the pores of the films because the polar functional groups, i.e., carbohydrates, tend to reorient toward the inner part of the cavities. Herein, based on the incompatibility of the homopolymer and the matrix and taking into account the initial hydrophobicity of the homopolymer employed, we will be able to immobilize proteins in hydrophobic regions.

EXPERIMENTAL SECTION

Materials. The amphiphilic block copolymer polystyrene-*b*-poly[poly(ethylene glycol) methyl ether methacrylate] (PS_{40}-*b*-$P(PEGMA300)_{48}$) (copolymer is labeled with the degree of polymerization of each block) and poly(2,3,4,5,6-pentafluorostyrene) ($P5FS_{21}$) were synthesized via atom transfer radical polymerization (ATRP) as previously reported.[15,21] High-molecular-weight polystyrene (Aldrich, $M_w = 2.50 \times 10^5$ g/mol) was used as polymeric matrix. Tetrahydrofuran (THF), dimethylsulfoxide (DMSO), triethylamine (TEA) and methanol (MeOH) were purchased from Scharlau. Sodium methanolate (MeONa) (25 wt % in methanol), 1-thio-β-D-glucose tetraacetate (GluOAc), chicken egg albumin and lectin-fluorescein isothiocyanate conjugate from *Canavalia ensiformis* (Con A-FITC) were supplied by Sigma-Aldrich. The buffer Trizma-HCl was also purchased from Aldrich. Sodium chloride (NaCl, Panreac), manganese chloride tetrahydrate ($MnCl_2$ $4H_2O$, 99%, Fluka), and calcium chloride dihydrate ($CaCl_2 \cdot 2H_2O$, 99.5%, Fluka) were added to the buffer for the molecular recognition. Round glass coverslips of 12 mm diameter were obtained from Ted Pella Inc. Water contact angles (CA) were measured using a KSV Theta goniometer. The volume of the droplets was controlled to be about 2.0 μL and a charge coupled device camera was used to capture the images of the water droplets for the determination of the contact angles.

Film Preparation. Polymer blend solutions were prepared by dissolving the PS matrix and the polymers in THF. Different ternary blends were studied varying the proportion of the components, as shown in Table 1. The total polymer concentration in all solutions was 30 mg/mL. Films were prepared from these solutions by casting onto glass wafers at room temperature under controlled humidity inside of a closed chamber.

Table 1. Chemical Composition of the Different Blends Used to Prepare the Microstructured Films

blend	PS (wt%)	PS_{40}-*b*-$P(PEGMA300)_{48}$ (wt %)	$P5SF_{21}$ (wt %)
B1	80	15	5
B2	80	10	10
B3	50	25	25

Film Modification. The films were immersed in a DMSO solution containing 10 mg/mL of GluOAc and 40 μL/mL of TEA and allowed to react overnight at room temperature. Then, the surface was rinsed both with DMSO and ethanol. Afterward, the deprotection of the acetate-protected thioglucose was carried out by treating the films with a solution of MeONa 10 wt % in methanol for 90 min and then washing them with methanol.

Lectin Interaction. To immobilize the protein, the surface was placed in a solution containing 1 mg/mL of Con A-FITC and 5 mg/mL of chicken egg albumin in a buffer solution (Trizma, pH 7.4, with 1 mM $MnCl_2$, 1 mM $CaCl_2$, and 0.1 M NaCl). After 30 min, the films were thoroughly rinsed with the buffer solution and distilled water and dried at room temperature.

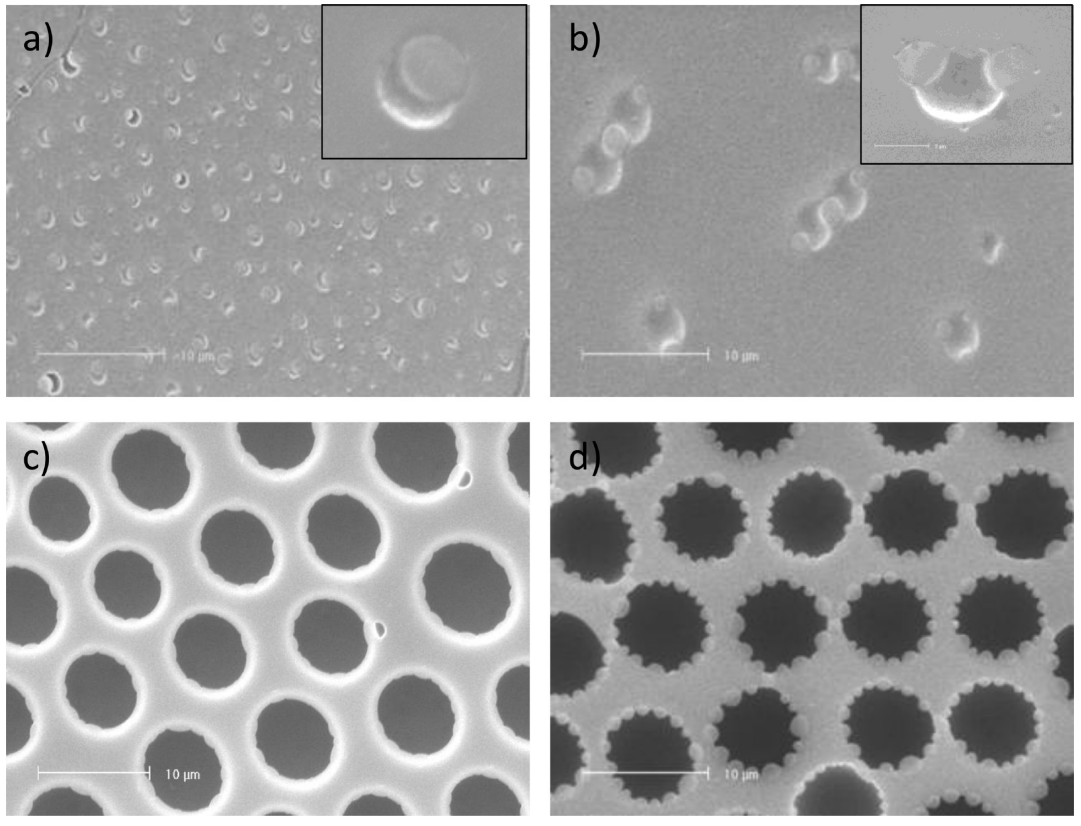

Figure 1. SEM images of films prepared from blend B1 with a polymer concentration of 30 mg/mL at (a) 20, (b) 50, (c) 70, and (d) 80% RH.

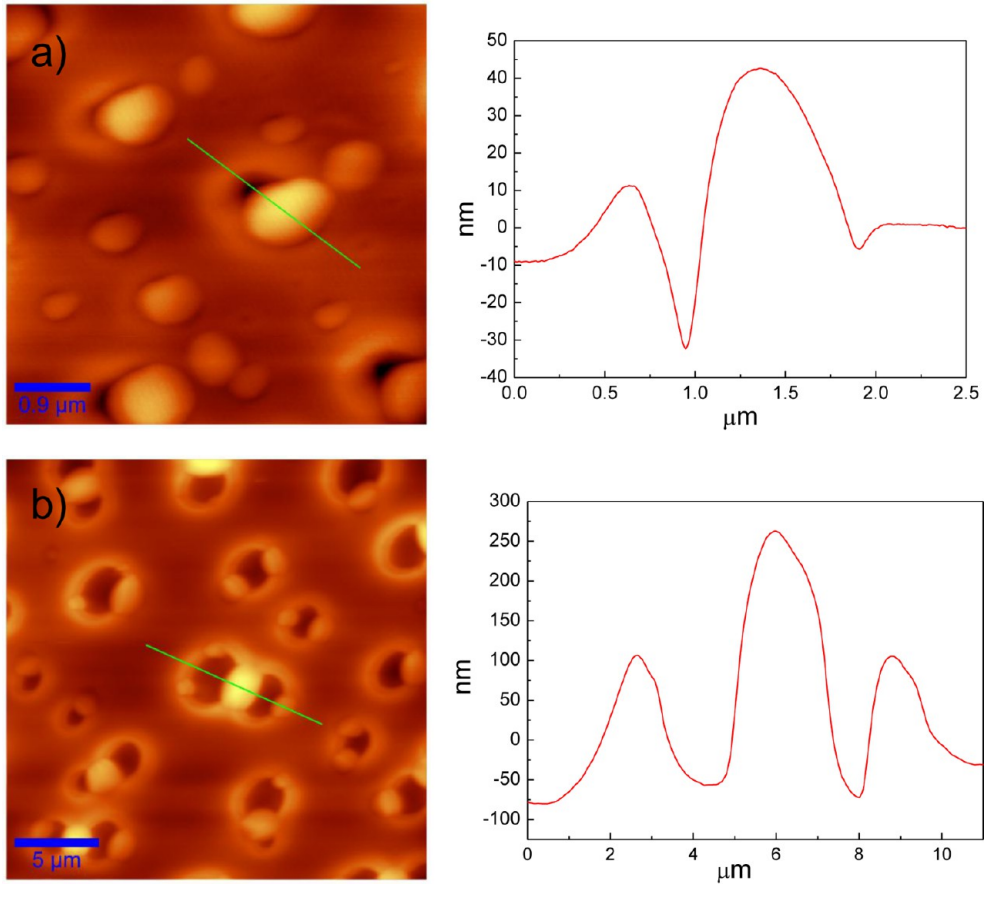

Figure 2. AFM height images and cross-sections of the polymer films of blend B1 prepared at (a) 20% and (b) 50% RH.

dx.doi.org/10.1021/am400679r | ACS Appl. Mater. Interfaces 2013, 5, 3943−3951

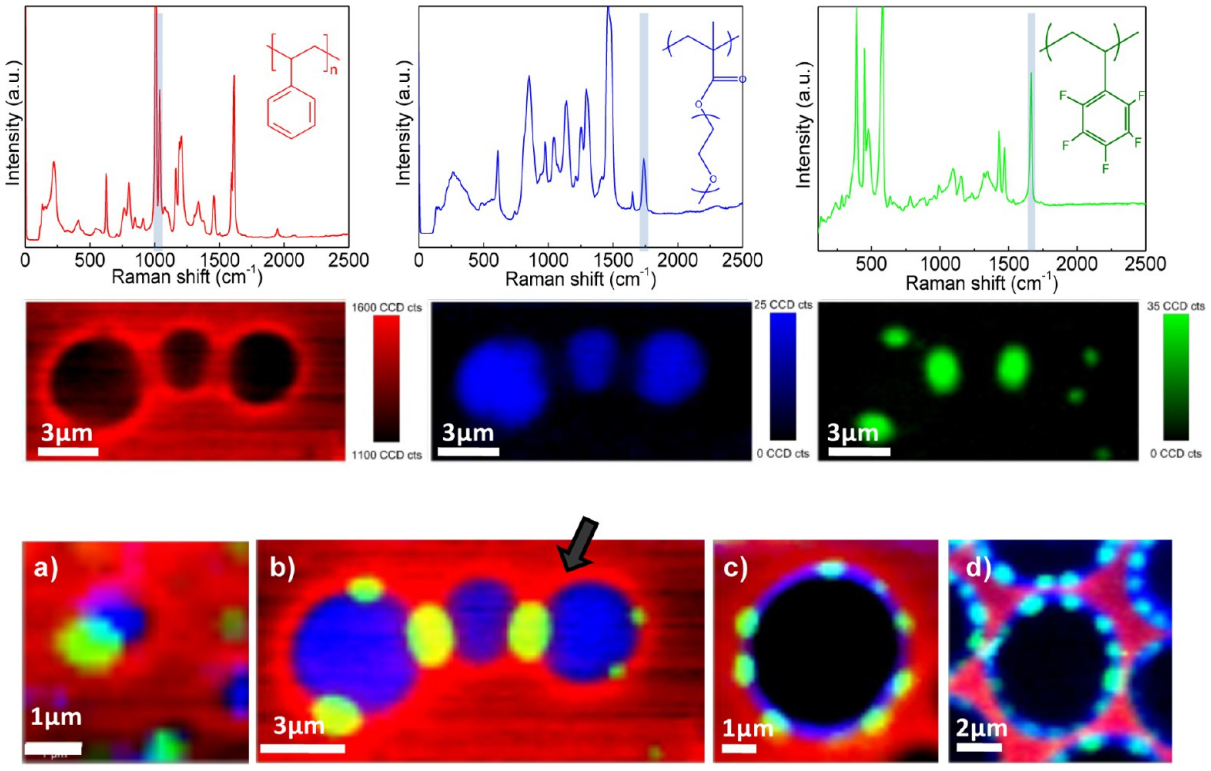

Figure 3. Above: Raman spectra of the components of the blend and their corresponding Raman maps for the film prepared from blend B1 at 50% RH. Red regions represent the higher intensity for the 1012 cm^{-1} associated with polystyrene while the integrated intensities of the Raman peaks at 1663 cm^{-1} for the P5FS and 1735 cm^{-1} associated with the P(PEGMA) are shown in a color green and blue color, respectively. Below: Raman micrographs constructed by merging the maps of the different components for films prepared from blend B1 at: (a) 20, (b) 50, (c) 70, and (d) 80% RH. An example of the construction is shown for b.

Measurements. Scanning electron microscopy (SEM) micrographs were taken using a Philips XL30 with an acceleration voltage of 25 kV. The samples were coated with gold–palladium (80/20) prior to scanning. The topography, chemical composition and distribution of the different components on the polymeric films were determined using confocal Raman microspectroscopy integrated with atomic force microscopy (AFM) on a CRM-Alpha 300 RA microscope (WITec, Ulm, Germany) equipped with Nd:YAG dye later (maximum power output of 50 mW power at 532 nm). An inverted fluorescence microscope (Nikon eclipse TE2000-S) was used to study the interaction of Con A-FITC with the polymer films. The images were captured with a Nikon Digital Sight DS-2MV camera.

RESULTS AND DISCUSSION

Initially, the ternary blend B1 (see Table 1) was prepared by mixing the amphiphilic block copolymer PS_{40}-*b*-P-$(PEGMA300)_{48}$ and the fluorinated homopolymer $P5FS_{21}$ with the PS matrix and dissolved in THF to obtain a 30 mg/mL solution. Several films were made by casting this polymer blend solution onto glass wafers under a moist atmosphere, varying the relative humidity (RH) from 20% to 80% in order to establish the effect of the humidity on the morphology of the films. The microstructures of the resulting polymer films were first observed by SEM, Figure 1. At low RH (20%), water condensation did not occur and the formation of porous films was not observed; however a certain roughness was detected at the surface. As can be seen in Figure 1a, the surface of the films displays a morphology consisting in shallow cavities near protrusions.

A careful examination of these films by AFM measurements (Figure 2) confirmed the presence of nondeep pores next to elevations. At higher humidity, 50%, the resulting film shows similar morphologies, but in this case the cavities are higher in diameter and a kind of "wormlike" structure is obtained (Figure 1b). The AFM topography images also reveal a "wormlike" morphology consisting in a sequence of protrusions alternating with holes. The structure observed by AFM additionally confirmed the SEM images indicating the formation of macrophase separated domains. This effect will be further analyzed by confocal Raman.

A typical porous film was obtained by increasing the relative humidity up to 70%. The diameter of the cavities and the density of pores augment significantly respect to the films prepared at 50% RH. Moreover, no evidence of secondary porosity was appreciated in the film that is sometimes observed in breath figures when amphiphilic block copolymers are used.[7−9] In this case, the SEM images show spherical protrusions placed on the edge of to the cavities forming intriguing microstructures. This morphology is more evident in the films prepared at 80% RH (Figure 1d). The size of the pore increases with the RH, presenting average diameters of 1.3 ± 0.3 μm, 2.7 ± 0.3 μm, 6.0 ± 1 μm, and 7.3 ± 0.4 μm for 20, 50, 70, and 80% RH, respectively. The regularity of the pores for the experiments that conduct to the formation of honeycomb patterns (70 and 80% RH) has been quantitatively analyzed by using the Voronoi analysis.[41] This analysis provides values defined in terms of entropy of conformation directly related to the regularity of the pore formation. Complementary to the visual order/disorder observed in the optical or SEM images, the Voronoi analysis is a more objective approach to quantify the pore order. The systems described herein have been analyzed from images with dimension of 60 × 80 μm^2, studying

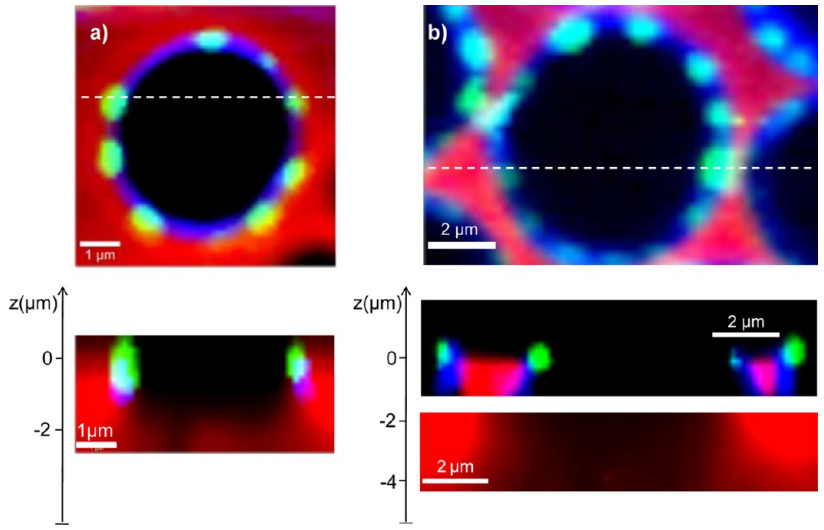

Figure 4. XY (above) and XZ (below) Raman mappings of films prepared from blend B1 at: (a) 70% and (b) 80% RH. Red areas correspond to high intensity of the 1012 cm^{-1} (PS), the blue areas are related to a high intensity of the 1735 cm^{-1} signal (P(PEGMA)), whereas the green domains correspond to a high intensity of the 1663 cm^{-1} signal (P5FS).

around 50 pores, giving conformational entropy values of 0.65 and 0.72, for the surfaces obtained at 70 and 80% RH, respectively. These two values are relatively low and much less than 1.71 for disordered random packing of pores, reflecting ordered hexagonal patterns.

The topography and surface morphology of these ternary blend films considerably differ from the reported blend in which a block copolymer containing a segment of PS compatible with the matrix was employed.[23] Because of the formation mechanism of the breath figures, the amphiphilic copolymer is expected to be arranged around the water droplets, inducing the orientation of hydrophilic P(PEGMA) blocks preferably inside the holes. On the other hand, the $P5FS_{21}$ homopolymer is expected to be located outside the holes on the outmost surface of the film due to the low surface energy of the fluorinated functional groups.[23] Further insight about the chemical composition of the micropatterned surfaces and the spatial distribution of the components of the blends was obtained by confocal Raman microscopy.

The images were taken point by point with a step of 100 nm, and performed using the ring breathing mode associated to PS and $P5FS_{21}$ (Raman shift at 1012 and 1663 cm^{-1}, respectively), and the strong band attributed to the carbonyl groups of the $P(PEGMA300)_{48}$ segment at 1735 cm^{-1}. Figure 3 shows the Raman spectra of the pure components contained in the blend and their corresponding Raman maps (i.e., the distribution of each component) for the film prepared from blend B1 at different RH. In the Raman micrographs it can be observed that, as expected, the amphiphilic copolymer PS_{40}-*b*-$P(PEGMA300)_{48}$ is preferentially located into the cavities. This is a consequence, as commented, of the segregation and orientation of the hydrophilic segments toward the water droplets during the solvent evaporation.[18,42−44] Concerning the fluorinated homopolymer, Raman mapping shows that the $P5FS_{21}$ is also segregated from the PS matrix and migrated selectively to the edges of the cavities. As expected, the $P5FS_{21}$ is not homogeneously distributed in the PS matrix, contrary to what was found in the case of the P5FS-*b*-PS block copolymer,[23] indicating a large incompatibility between these three components. Morphologies displayed in panels a and b in Figure 3 exhibit similar features, i.e., macrophase separation between the components. This result is in good agreement with previous studies concerning ternary polymer blends consisting of three incompatible polymers with high and identical values of binary interaction parameters.[45−47] Those structures typically resulted from the spinodal decomposition of ternary polymer blends, where the phase corresponding to the PS matrix is the continuous phase (red) while the phases associated to $P5FS_{21}$ (green) and PS_{40}-*b*-$P(PEGMA300)_{48}$ (blue) are dispersed forming spherical domains at low RH. However, in this particular case the process of formation and distribution of the components on the polymer surface is far from being random. In effect, the breath figures process strongly affects the segregation of the different polymer phases. Thus, controlling the ambient humidity during the film formation, the surface morphology and the distribution of the blend components can be significantly modified. Previous works on the formation of surface patterns using ternary blends focused on the influence of the proportion of the different components within the blend on the surface morphology.[45] Herein, we explored the effect of the relative humidity while maintaining the same blend composition. The RH is directly related with the amount of condensed water vapor and thus the dimensions of the water droplets formed on the surface morphology. As depicted in panels c and d in Figure 3, an increase of the RH favors the formation of regular pores and evidence the segregation and migration of the polar copolymer, PS_{40}-*b*-$P(PEGMA300)_{48}$ toward the inner part of the pore. This behavior has been previously observed and is well-understood.[18,40−42] In addition, the distribution of this component within the pore is not usual (see cross-sectional profiles in Figure 4). In the honeycomb studies reported up to date, the amphiphilic copolymer is homogeneously distributed within the pore. In this case, by focusing on the cross-section profile image, we observed that the copolymer is concentrated on the top area of the pore. This effect has been observed previously by our group in breath figures and it has been associated with the coffee stain effect. This effect is related to the solubility of the block copolymer within the condensing water droplets. In effect, during solvent evaporation, the water droplets formed at

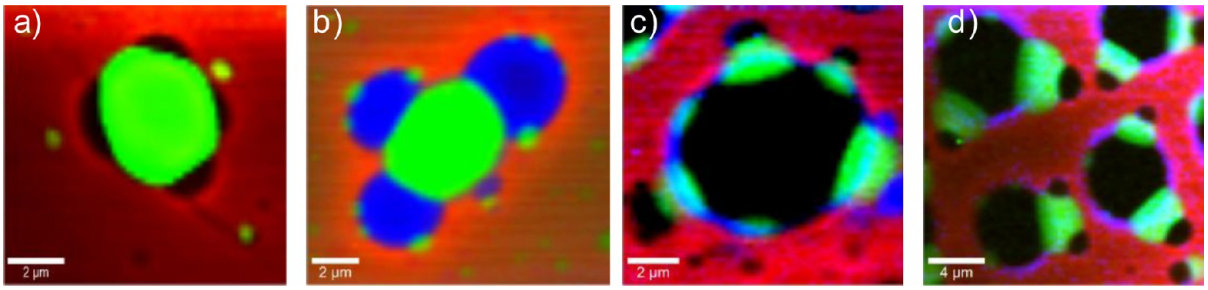

Figure 5. Raman micrographs of the films prepared from blend B2 at: (a) 20, (b) 50, (c) 70, and (d) 80% RH. Red areas correspond to high intensity of the 1012 cm^{-1} related to the presence of PS, the blue areas are related to a high intensity of the 1735 cm^{-1} signal associated to the P(PEGMA) block and the green domains correspond to a high intensity of the 1663 cm^{-1} signal assigned to the P5FS homopolymer.

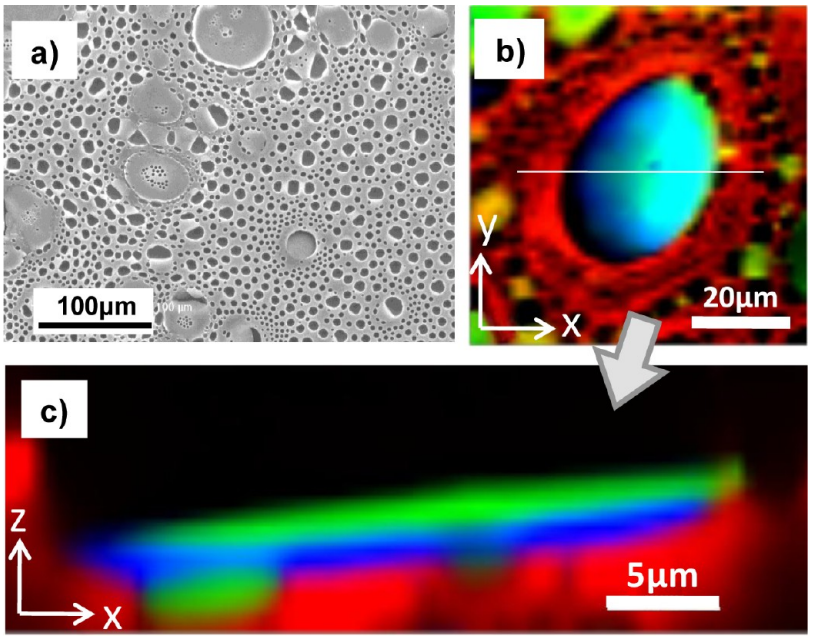

Figure 6. (a) SEM image, (b) XY Raman micrograph, and (c) XZ cross-section Raman mapping of a film prepared from B3 and casted at 70% RH. Red areas correspond to high intensity of the 1012 cm^{-1} (PS), the blue areas are related to a high intensity of the 1735 cm^{-1} signal (P(PEGMA)), whereas the green domains correspond to a high intensity of the 1663 cm^{-1} signal (P5FS).

the solvent/air interface solubilize the amphiphilic block copolymer. When the volatile solvent is evaporated, the water droplets present at the polymer/air interface, partially embedded in the polymer, start to evaporate. This evaporation occurs from the edge of the pore and a convective process induced the enrichment of the pore edge in block copolymer.

The particular design of this blend containing a homopolymer includes additional unprecedented properties. As can be observed in panels c and d in Figure 3, at high relative humidity, "necklacelike" microstructures around the pore were observed. These structures proceed from the $P5FS_{21}$ homopolymer which is also located on the edges forming spherical domains with relative narrow polydisperse sizes (1.00 ± 0.25 μm). This observation could be explained considering both the incompatibility between the homopolymer and the other two components and the low surface energy of the fluorinated homopolymer which makes it migrate toward the surface of the film.[45−48]

As a result, by using this particular ternary blend, the pore contains simultaneously two antagonist functionalities, i.e., hydrophilic and hydrophobic functional groups, whereas the interpore surface is constituted exclusively by PS.

In addition, the variation of the blend composition can also contribute to vary the surface morphology and topography while maintaining the same RH. Therefore, the composition of the blend was modified by increasing the amount of $P5FS_{21}$ in the blend up to 10 wt % and simultaneously decreasing the content of PS_{40}-*b*-$P(PEGMA300)_{48}$ until 10 wt % (sample B2, Table 1). Raman micrographs depicted in Figure 5 show relatively similar patterns as those found for blend B1 (Figure 3). However in this case, the increment of the $P5FS_{21}$ proportion while diminishing the PS_{40}-*b*-$P(PEGMA300)_{48}$ content, entails an increase in size of the $P5FS_{21}$ domains related to the polar regions. At high RH the resulting micropores present large $P5FS_{21}$ domains around their edges connecting with smaller cavities.

Furthermore, the decrease of PS matrix, accompanied by the augment of minority short-length polymers (blend B3, Table 1) provokes the formation of large and irregular macrophase separation in the investigated RH range (20−80%), as shown in Figure 6. XZ image confirms that the $P5FS_{21}$ tends to migrate toward the air interface to minimize the surface tension of the film.

Scheme 1. Schematic Representation of the Approach Employed to Incorporate Glucose Moieties and, Subsequently, Con A onto the Microstructured Films

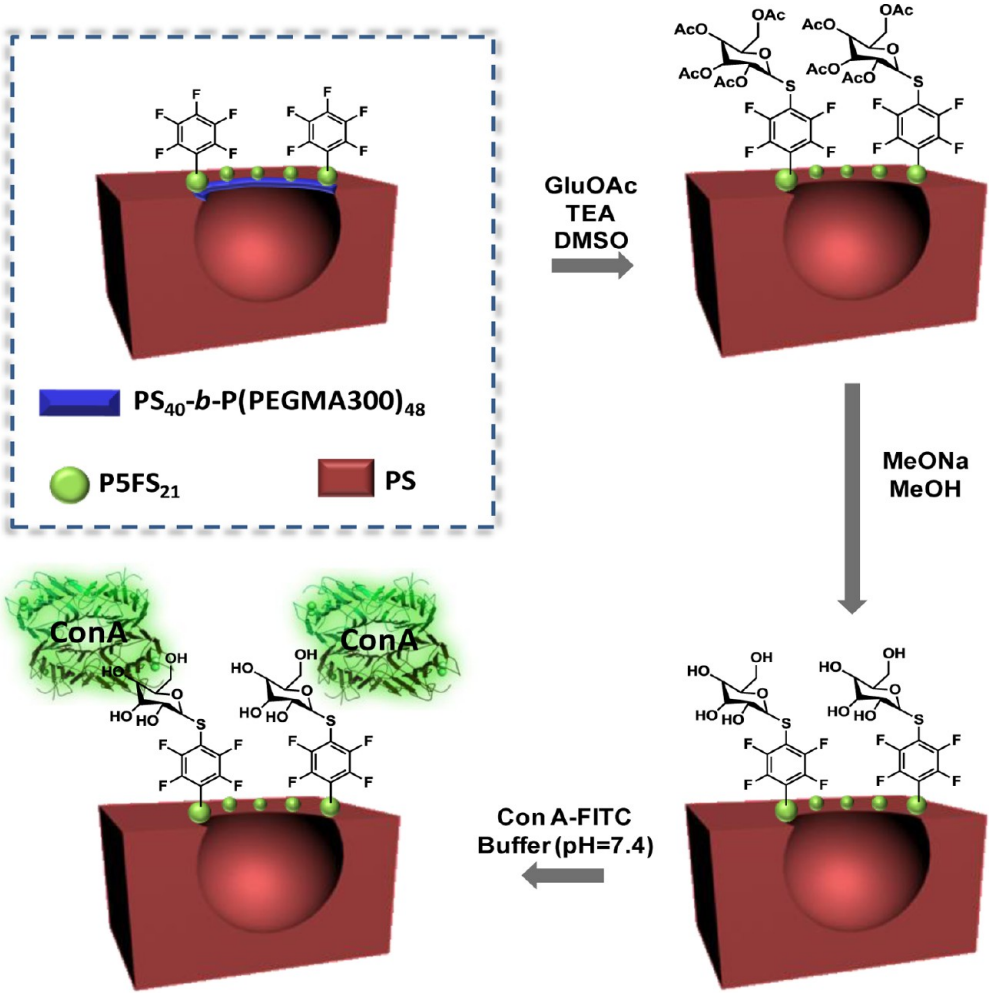

Therefore, employing blends with a relatively low amount of the minority polymers PS_{40}-*b*-$P(PEGMA300)_{48}$ and $P5FS_{21}$ (20 wt %) with respect the PS matrix (80 wt %) and depending on the casting ambient conditions (for instance, the relative humidity) different multifunctional and microstructured patterns were obtained.

Particularly interesting are the surfaces obtained from blends B1 and B2 at high RH in which the separated functionalities, hydrophilic and hydrophobic, within the pore inner wall can be selectively modified chemically. In order to illustrate the possibilities to further modify the surface chemistry, the films prepared from blend B1 containing 80 wt % PS matrix and 5 wt % fluorinated homopolymer, were utilized to immobilize glucose moieties which are extensively reported to serve as model to test the lectin-binding ability. For that purpose the thiol-*para*-fluorine "click" reaction approach (Scheme 1) was employed.

As previously demonstrated by Raman microscopy, the fluorinated homopolymer is located preferentially on the edge the pores, forming spherical domains. Thus, the active groups, that is, the labile *para*-fluorine substituents of pentafluorostyrene, are segregated forming a special pattern at the surface of the film. The carbohydrate moieties were anchored to the fluorinated domains by the so-called thiol-*para*-fluorine "click" reaction. Using this reaction, an acetyl β-D-thioglucopyranose is attached onto pentafluorostyrene via a nucleophilic substitution of *para*-fluorine, followed by the deprotection of the acetyl-protected thioglucose. The "click" reaction was carried out at room temperature in DMSO using an excess of thioglucose (5FS/GluOAc ratio of 14/1). Under those conditions the acetyl-protected thioglucose is soluble in DMSO whereas the polystyrene matrix and the fluorinated homopolymer are insoluble. On the contrary, the amphiphilic block copolymer PS_{40}-*b*-$P(PEGMA300)_{48}$ is soluble in the DMSO solvent. The films were immersed in DMSO to investigate how the reaction medium would affect the surface structure. The XY and XZ micro-Raman mappings (Figure 7) show that the PS_{40}-*b*-$P(PEGMA300)_{48}$ was removed from the surface of the films. Nevertheless, the microstructure of the film was maintained and the fluorinated domains remained apparently intact.

Despite the removal of the amphiphilic copolymer by the reaction medium, it has to be mentioned that the addition of this amphiphilic copolymer to the blend is necessary to create these particular microstructures because it participates in the breath figures process stabilizing the condensed water droplets. After the "click" reaction, the films were analyzed again by Raman microscopy. However, the sensibility of this technique was not enough to detect the glucose molecules attached to the surface probably because the coupling reaction affords the immobilization of only a glucose monolayer on the outermost

dx.doi.org/10.1021/am400679r | ACS Appl. Mater. Interfaces 2013, 5, 3943−3951

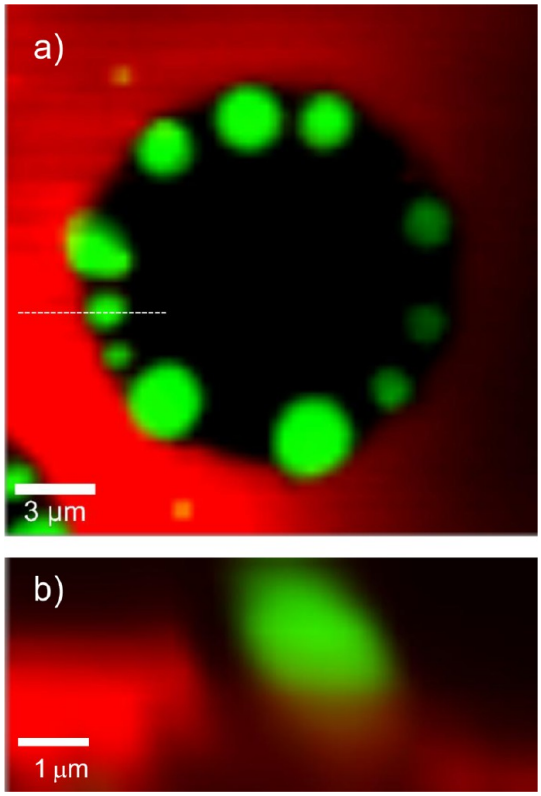

Figure 7. Raman micrographs of films prepared from blend B1 at 70% RH after the treatment in DMSO: (a) XY and (b) XZ mappings. Red areas correspond to high intensity of the 1012 cm^{-1} (PS), whereas the green domains correspond to a high intensity of the 1663 cm^{-1} signal (P5FS).

surface of the fluorinated domains. As an alternative to characterizing the success of the reaction we employed fluorescence spectroscopy. In effect, this porous and microstructured film was used as template to decorate the fluorinated spherical structures with fluorescent labeled proteins that recognize the immobilized glucose moieties. The potential of these films to guide the patterning of proteins was analyzed using Concanavalin A, which is a specific lectin for binding both glucose and mannose residues. A fluorescently labeled (FITC) Con A that can be easily detected by fluorescence techniques was employed. The surface was immersed in a solution of Con A-FITC (1 mg/mL) and Chicken egg albumin (5 mg/mL) in a buffer Trizma solution of pH 7.4 for 30 min, followed by a standard washing step. The albumin is generally used for blocking solid surface, avoiding in this way the nonspecific interaction between the polystyrene matrix and the Con A. Fluorescence microscopy was utilized to determine the Con A attachment to the surface. As can be seen in Figure 8, the fluorescence is detected only around the holes, in the $P5FS_{21}$ spherical domains, indicating the location of the glucose moieties which are specifically recognized by the protein, evidencing the success of the "click" reaction to postfunctionalize the breath figures patterns. Furthermore, a sample employed as control experiment in which no postmodification steps were carried out, and therefore, no-binding glucose molecules are available and did not show any fluorescence at all.

The surface modification was additionally followed by contact angle measurements and the variations of the contact angle depending on the surface treatment have been included in Figure 9. Whereas the films obtained upon solvent casting,

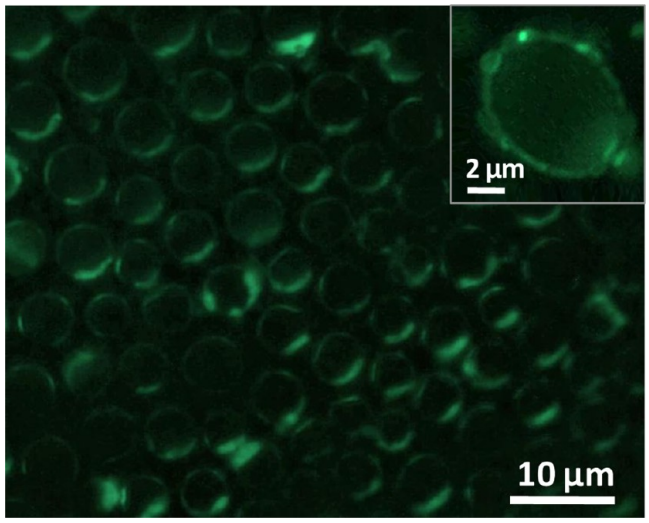

Figure 8. Top view fluorescence images after the incubation with Con A-FITC of porous films prepared from blend B1 at 80% RH modified with 1-thio-β-D-glucose tetraacetate via "click" chemistry and then deprotected.

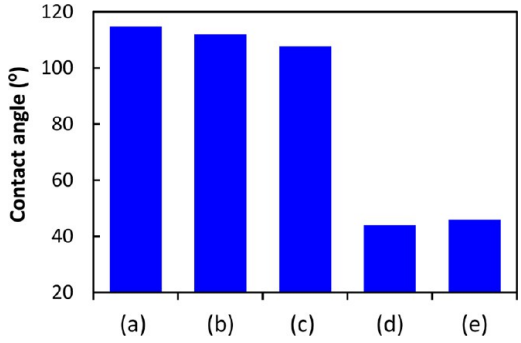

Figure 9. Contact angle measurements of porous films prepared from blend B1 at 80% RH: (a) unmodified film, (b) film treated with DMSO, (c) after "click" reaction with 1-thio-β-D-glucose tetraacetate, (d) upon deprotection of the acetyl groups of the glucose, and (e) after incubation with Con A-FITC.

treated with DMSO or after chemical reaction exhibit contact angle values between 107 and 114°, the deprotection of the acetyl groups of the films modified by click chemistry with 1-thio-β-D-glucose tetraacetate decreased significantly the contact angle observed. This fact clearly indicates the presence of deprotected glucose at the surface of the films. In addition, after the recognition experiment with Con A, similar contact angles were observed, showing both that the protein is anchored at the surface by means of glucose and that glucose has not been removed from the surface during the treatment.

CONCLUSIONS

In summary, microstructured surfaces with variable morphology and chemical composition are easily and rapidly prepared in one single step by the combination of breath figures and phase separation processes. The surfaces are obtained from solutions of ternary blends consisting of a high molecular weight polystyrene matrix, an amphiphilic copolymer, PS_{40}-*b*-$P(PEGMA300)_{48}$, and a fluorinated homopolymer, $P5FS_{21}$. Unprecedented ordered patterns are obtained where the microstructures can be tuned varying both the composition of the blend and the relative humidity. These studies also reveal

the importance of the incompatibility between the different components of the blend in the formation process of the film and, hence, on the final microstructure. As a result, hydrophilic and hydrophobic functional groups can decorate the inner part of the pore. The ordered porous films can be chemically modified for instance by using click chemistry. Thiol-*para*-fluorine "click" reaction was employed to covalently attach glucose moieties specifically to the spherical fluorinated domains. Then, the ability of the immobilized glucose to recognize Concanavalin A enables the creation of protein micropatterns by a nonlithografic method.

Moreover, the use of polymeric blends in the breath figures technique entails the participation of the phase separation process. The combination of both processes opens a huge variety of creating multifunctional and microstructured patterns. As demonstrated, varying the experimental conditions employed to fabricate the films such as the relative humidity or blend composition, the morphology of the surface and thus, the pattern of proteins can be tuned. Therefore, this method exemplifies a versatile and potent possibility to design different surfaces with controlled topography and compositional distribution.

AUTHOR INFORMATION

Corresponding Author

*E-mail: jrodriguez@ictp.csic.es (J.R-H.); sbonilla@ictp.csic.es (A.M-B.).

Notes

The authors declare no competing financial interest.

ACKNOWLEDGMENTS

This work was financially supported by the MINECO (Projects MAT2010-17016, MAT2010-21088-C03-01, and COST Action MP0904 SIMUFER). A M.-B. gratefully acknowledges the MINECO for her Juan de la Cierva postdoctoral contract and A.S.d.L. thanks the Ministerio de Educación for his FPU predoctoral fellowship.

REFERENCES

(1) Li, L.; Chen, C.; Li, J.; Zhang, A.; Liu, X.; Xu, B.; Gao, S.; Jin, G.; Ma, Z. *J. Mater. Chem.* **2009**, *19*, 2789−2796.
(2) Connal, L. A.; Franks, G. V.; Qiao, G. G. *Langmuir* **2010**, *26*, 10397−10400.
(3) Akolekar, D. B.; Hind, A. R.; Bhargava, S. K. *J. Colloid Interface Sci.* **1998**, *199*, 92−98.
(4) Deutsch, M.; Vlasov, Y. A.; Norris, D. J. *Adv. Mater.* **2000**, *12*, 1176−1180.
(5) Widawski, G.; Rawiso, M.; François, B. *Nature* **1994**, *369*, 387−389.
(6) Srinivasarao, M.; Collings, D.; Philips, A.; Patel, S. *Science* **2001**, *292*, 79−83.
(7) Bunz, U. H. F. *Adv. Mater.* **2006**, *18*, 973−989.
(8) Hernandez-Guerrero, M.; Stenzel, M. H. *Pol. Chem.* **2012**, *3*, 563−577.
(9) Escalé, P.; Rubatat, L.; Billon, L.; Save, M. *Eur. Polym. J.* **2012**, *48*, 1001−1025.
(10) Ferrari, E.; Fabbri, P.; Pilati, F. *Langmuir* **2011**, *27*, 1874−1881.
(11) Angus, S. D.; Davis, T. P. *Langmuir* **2002**, *18*, 9547−9553.
(12) Tian, Y.; Dai, C.; Ding, H.; Jiao, Q.; Wang, L.; Shi, Y.; Liu, B. *Polym. Int.* **2007**, *56*, 834−839.
(13) Wong, K. H.; Davis, T. P.; Barner-Kowollik, C.; Stenzel, M. H. *Polymer* **2007**, *48*, 4950−4965.
(14) De León, A. S.; Muñoz-Bonilla, A.; Fernández-García, M.; Rodríguez-Hernández, J. *J. Polym. Sci., Polym. Chem.* **2012**, *50*, 851−859.
(15) Muñoz-Bonilla, A.; Van Herk, A. M.; Heuts, J. P. A. *Macromolecules* **2010**, *43*, 2721−2731.
(16) Stenzel-Rosenbaum, M. H.; Davis, T. P.; Fane, A. G. *Angew. Chem., Int. Ed.* **2001**, *40*, 3428−3432.
(17) Galeotti, F.; Calabrese, V.; Cavazzini, M.; Quici, S.; Poleunis, C.; Yunus, S.; Bolognesi, A. *Chem. Mater.* **2010**, *22*, 2764−2769.
(18) Stenzel, M. H.; Barner-Kowollik, C.; Davis, T. P. *J. Polym. Sci., Polym. Chem.* **2006**, *44*, 2363−2375.
(19) Kon, K.; Brauer, C. N.; Hidaka, K.; Löhmannsröben, H. G.; Karthaus, O. *Langmuir* **2010**, *26*, 12173−12176.
(20) Li, X.; Zhang, L.; Wang, Y.; Yang, X.; Zhao, N.; Zhang, X.; Xu, J. *J. Am. Chem. Soc.* **2011**, *133*, 3736−3739.
(21) Muñoz-Bonilla, A.; Ibarboure, E.; Papon, E.; Rodriguez-Hernandez, J. *J. Polym. Sci., Polym. Chem.* **2009**, *47*, 2262−2271.
(22) Munoz-Bonilla, A.; Ibarboure, E.; Bordege, V.; Fernandez-Garcia, M.; Rodriguez-Hernandez, J. *Langmuir* **2010**, *26*, 8552−8558.
(23) De León, A. S.; Del Campo, A.; Fernández-García, M.; Rodríguez-Hernández, J.; Muñoz-Bonilla, A. *Langmuir* **2012**, *28*, 9778−9787.
(24) Yabu, H.; Shimomura, M. *Langmuir* **2006**, *22*, 4992−4997.
(25) Yabu, H.; Hirai, Y.; Shimomura, M. *Langmuir* **2006**, *22*, 9760−9764.
(26) Kojima, M.; Yabu, H.; Shimomura, M. *Macromol. Symp.* **2008**, *267*, 109−112.
(27) Boker, A.; Lin, Y.; Chiapperini, K.; Horowitz, R.; Thompson, M.; Carreon, V.; Xu, T.; Abetz, C.; Skaff, H.; Dinsmore, A. D.; Emrick, T.; Russell, T. P. *Nat. Mater.* **2004**, *3*, 302−306.
(28) Kolb, H. C.; Finn, M. G.; Sharpless, K. B. *Angew. Chem., Int. Ed.* **2001**, *40*, 2004−2021.
(29) Kempe, K.; Krieg, A.; Becer, C. R.; Schubert, U. S. *Chem. Soc. Rev.* **2012**, *41*, 176−191.
(30) Slavin, S.; Burns, J.; Haddleton, D. M.; Becer, C. R. *Eur. Polym. J.* **2011**, *47*, 435−446.
(31) Binder, W. H.; Sachsenhofer, R. *Macromol. Rapid Commun.* **2007**, *28*, 15−54.
(32) Becer, C. R.; Hoogenboom, R.; Schubert, U. S. *Angew. Chem., Int. Ed.* **2009**, *48*, 4900−4908.
(33) Babiuch, K.; Wyrwa, R.; Wagner, K.; Seemann, T.; Hoeppener, S.; Becer, C. R.; Linke, R.; Gottschaldt, M.; Weisser, J. r.; Schnabelrauch, M.; Schubert, U. S. *Biomacromolecules* **2011**, *12*, 681−691.
(34) Samaroo, D.; Vinodu, M.; Chen, X.; Drain, C. M. *J. Comb. Chem.* **2007**, *9*, 998−1011.
(35) Geijtenbeek, T. B. H.; Kwon, D. S.; Torensma, R.; Van Vliet, S. J.; Van Duijnhoven, G. C. F.; Middel, J.; Cornelissen, I. L. M. H. A.; Nottet, H. S. L. M.; KewalRamani, V. N.; Littman, D. R.; Figdor, C. G.; Van Kooyk, Y. *Cell* **2000**, *100*, 587−597.
(36) Tirrell, D. A. *Nature* **2004**, *430*, 837.
(37) Min, E.; Wong, K. H.; Stenzel, M. H. *Adv. Mater.* **2008**, *20*, 3550−3556.
(38) Zhang, Y.; Wang, C. *Adv. Mater.* **2007**, *19*, 913−916.
(39) Ke, B.-B.; Wan, L.-S.; Xu, Z.-K. *Langmuir* **2010**, *26*, 8946−8952.
(40) Min, E. H.; Ting, S. R. S.; Billon, L.; Stenzel, M. H. *J. Polym. Sci., Polym. Chem.* **2010**, *48*, 3440−3455.
(41) Limaye, A. V.; Narhe, R. D.; Dhote, A. M.; Ogale, S. B. *Phys. Rev. Lett.* **1996**, *76*, 3762−3765.
(42) Billon, L.; Manguian, M.; Pellerin, V.; Joubert, M.; Eterradossi, O.; Garay, H. *Macromolecules* **2009**, *42*, 345−356.
(43) Stenzel, M. H.; Davis, T. P. *Aust. J. Chem.* **2003**, *56*, 1035−1038.
(44) Wong, K. H.; Davis, T. P.; Bamer-Kowollik, C.; Stenzel, M. H. *Polymer* **2007**, *48*, 4950−4965.
(45) Nauman, E. B.; He, D. Q. *Polymer* **1994**, *35*, 2243−2255.
(46) Sprenger, M.; Walheim, S.; Budkowski, A.; Steiner, U. *Inter. Sci.* **2003**, *11*, 225−235.
(47) Huang, C.; Olvera De La Cruz, M.; Swift, B. W. *Macromolecules* **1995**, *28*, 7996−8005.
(48) Iyengar, D. R.; Perutz, S. M.; Dai, C. A.; Ober, C. K.; Kramer, E. J. *Macromolecules* **1996**, *29*, 1229−1234.